INT. J. NUM. METH. HEAT FLUID FLOW, VOL. 5, 705–716 (1995)

NUMERICAL VISUALIZATION OF CONVECTIVE HEAT TRANSFER FROM A SPHERE – WITH AND WITHOUT RADIAL MASS EFFLUX

HIMADRI CHATTOPADHYAY† AND SUKANTA K. DASH‡

† *Thermal and Fluid Engineering Group, Central Mechanical Engineering Research Institute, Durgapur-713 209, India*
‡ *Lehrstuhl für Strömungsmechanik, Friedrich-Alexander-Universität, Erlangen-Nürnberg, 91058 Erlangen, Germany*
† *R & D Division, TISCO, Jamshedpur 831007, India*

ABSTRACT

The conception of a heat function, just like the stream function used in a laminar two dimensional incompressible flow field visualization, has been introduced to visualize the convective heat transfer or the flow of energy around a sphere when the sphere is either being cooled or heated by a stream of fluid flowing around it. The heat function is developed in a spherical polar coordinate and is used to generate the heat lines around the sphere. The heat lines essentially show the magnitude and direction of energy transfer around the sphere with and without the existence of a finite radial velocity at the surface. The steady state hydrodynamic field around the sphere is numerically obtained up to a maximum Reynolds number of 100 and the corresponding thermal field has been obtained by solving the steady state energy equation. The field properties thus obtained are utilized to form the heat function, which becomes an effective tool for visualization of convective heat transfer.

KEY WORDS Numerical visualization Sphere Convective heat transfer Heat function Heat line

NOMENCLATURE

a'	Radius of the sphere
C	Specific heat
C_D	Drag coefficient
H'	Heat function
H	Non-dimensional heat function (Eq. 12)
k	Thermal conductivity
Nu	Nusselt number
Pe	Peclet number ($2U_\infty a'/\alpha$)
Pr	Prandtl number (ν/α)
Re	Reynolds number ($2U_\infty a'/\nu$)
r'	Radial co-ordinate
r	Non-dimensional r (r'/a')
T'	Temperature
T_i'	Initial sphere temperature
T_∞'	Free stream temperature
T	Non-dimensional temperature (T'/T_i')
U_∞	Free stream velocity
V'	Velocity
V_s'	Radial velocity at sphere surface
V'	Non-dimensional velocoty (V'/U_∞)
α	Thermal diffusivity
ψ'	Stream finction
ψ	Non-dimensional stream function ($\psi'/(U_\infty a'^2)$)
ν	Kinematic viscosity
ρ	Density
θ	Azimuthal co-ordinate
ζ'	Vorticity function
ζ	Non-dimensional vorticity function ($\zeta' a'/U_\infty$)

Subscript

i	At the initial stage
r	Radial component
θ	Azimuthal component

0961–5539/95/070705–11$2.00

Received January 1994
Revised July 1994

INTRODUCTION

Flow visualization by experimentation has become a very important tool to 'see' the flow pattern in complex geometries where flow field solution by numerical methods is still a non-trivial problem. In such cases, experiments have helped tremendously to understand the behaviour of the flow field and hence the physical situation. A straight flow visualization technique gives enough impression of the local velocity field but it has to be photographed for future reference and further study. The development of stream function has helped engineers to see the flow field as and when required, by numerically generating the stream lines in a flow field. As the tangent to the stream lines give the direction of velocity at that point, a family of stream lines essentially present a 'bird's eye' view of the entire flow field in two dimension. But they do not give any direct impression regarding the magnitude of the velocity at any point. Moreover, development of stream lines for three dimensional flow is not possible. Thus the conception of stream lines is limited to two dimensional incompressible flow situations. But recently, because of higher graphics handling capabilities of computers, it has become popular to represent the flow field by velocity vector plots as a means of numerical flow visualization. In this regard, nothing stands comparable to velocity vector plots in the flow domain. These give a quantitative idea of the local velocity along with its direction.

An understanding of the flow field helps to analyze the heat transfer characteristics in it, for which flow visualization is so important in the field of heat transfer. But the use of an efficient tool for direct visualization of heat transfer is not found except the visualization of isotherms which is only meaningful in case of pure conduction heat transfer where the flow of energy is locally orthogonal to the isotherms. But isotherms fail to represent the flow of energy in convective heat transfer because in convection, there are two parts of energy transfer, one through convection ($\rho C_p UT$) and the other conduction ($-\kappa \partial T/\partial X$). It was Bejan who felt the need to develop a proper tool for visualizing convective heat transfer and suggested the use of a heat function. He has developed a heat function which is capable of representing the convection heat transfer in a cartesian coordinate system[1,2]. Like the stream lines, heat lines are locally parallel to the direction of energy flow, hence energy flow does not cross any heat line. It is believed that the heat function is a proper tool for energy flow visualization in a convective medium and there will be more discussions on it in the present work.

The main objective of the present work is to generate methodology to develop a heat function (following the work of Kimura and Bejan[1]) for a spherical polar coordinate system, which can generate heat lines to show the energy flow around a sphere when the sphere is either being cooled or heated by the surrounding fluid stream. For this purpose the flow field around a sphere is solved for various Reynolds number (to a maximum of 100) and then the steady state energy equation has been solved to predict the temperature field. The effect of radial mass efflux from the surface of the sphere, has also been taken into consideration for visualizing the energy flow around it. The predicted velocity and temperature fields help to generate the heat function, which is found to be a very effective tool for visualizing convective heat transfer.

STATEMENT OF THE PROBLEM

Consider a solid spherical particle of radius a', having an initial temperature T_i', which is suddenly immersed in an unbounded laminar flow with a temperature of T_∞' (*Figure 1*). It is assumed that, far away from the sphere, the free stream temperature remains fixed at T_∞'. It is also assumed that the flow field around the particle is axisymmetric (symmetric in ϕ) and steady; the fluid velocity U_∞ is uniform far from the sphere. If $T_\infty' > T_i'$ then the sphere is being heated by the surrounding flow, otherwise the sphere is being cooled. The heat conductance and the heat capacity ratio of the sphere to that of the surrounding fluid $(\rho C)_{sphere}/(\rho C)_{fluid}$ is assumed to be so high that its bulk temperature does not change with time and also there exists no temperature

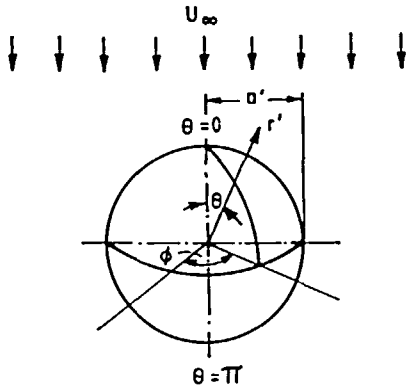

Figure 1 System of co-ordinates and nomenclature used in the theoretical analysis

gradient within it. The above assumption is reasonable only for metallic spheres in a gaseous or liquid environment. Theoretically, if $(\rho C)_{fluid}/(\rho C)_{sphere}$ is zero, then the bulk temperature of the sphere never changes with time. For instance, the heat capacity ratio of air to that of a nickel sphere is 0.00016 and to that of an iron sphere is 0.00034. These values are practically very low to keep the sphere at a constant temperature of T_i, i.e. at the initial temperature of the sphere. Hence the temperature field around the sphere is assumed to be steady and like the flow field the temperature field is also assumed to be axisymmetric. The free stream temperature, T_∞ is assumed to be low such that the energy interaction due to radiation can be neglected. It is intended to visualize the convective heat transfer from the sphere for the above situation.

Governing equations

The flow field around the sphere can be expressed by the steady, axisymmetric incompressible Navier–Stokes equation in the form of non-dimensional stream function and vorticity as[3,4]:

$$\frac{Re}{2}\left[\frac{\partial\psi}{\partial r}\frac{\partial}{\partial\theta}\left(\frac{\zeta}{r\sin\theta}\right)-\frac{\partial\psi}{\partial\theta}\frac{\partial}{\partial r}\left(\frac{\zeta}{r\sin\theta}\right)\right]\sin\theta = E^2(E^2\psi) \tag{1}$$

$$E^2\psi = \zeta r\sin\theta \tag{2}$$

where

$$E^2 = \frac{\partial^2}{\partial r^2}+\frac{\sin\theta}{\partial r^2}\frac{\partial}{\partial r}\left(\frac{1}{\sin\theta}\frac{\partial}{\partial\theta}\right) \tag{3}$$

The radial and tangential velocity components at any point in the flow field can be obtained from (4) and (5):

$$V_r = -\frac{1}{r^2\sin\theta}\frac{\partial\psi}{\partial\theta} \tag{4}$$

$$V_\theta = \frac{1}{r\sin\theta}\frac{\partial\psi}{\partial r} \tag{5}$$

The steady state convective heat transfer from the sphere is governed by the following

dimensionless energy equation for the fluid[5,6]:

$$\frac{Pe}{2}\left[V_r\frac{\partial T}{\partial r}+\frac{V_\theta}{r}\frac{\partial T}{\partial \theta}\right]=\frac{1}{r^2}\frac{\partial}{\partial r}\left(r^2\frac{\partial T}{\partial r}\right)+\frac{1}{r^2\sin\theta}\frac{\partial}{\partial\theta}\left(\sin\theta\frac{\partial T}{\partial\theta}\right) \tag{6}$$

As the main objective of the present work is to visualize the convective heat transfer, we will now proceed to formulate the '*Heat Function*' H. In convection, the transport of energy through the flow field is a combination of both thermal diffusion and enthalpy flow. For any such field the heat function $H'(r', \theta')$ can be defined such that the net flow of energy (sum of thermal diffusion and enthalpy flow) across each $H' =$ constant line is zero. The mathematical definition of the *Heat function, H'*, follows in the steps of (4) and (5) if, this time, the aim is to satisfy the energy equation. For a steady state convection through a constant property homogeneous fluid[1,7] the energy equation in the spherical polar coordinate is:

$$\left[V_r'\frac{\partial T'}{\partial r'}+\frac{V_\theta'}{r'}\frac{\partial T'}{\partial\theta}\right]=\frac{\alpha}{r'^2}\frac{\partial}{\partial r'}\left(r'\frac{2\partial T'}{\partial r'}\right)+\frac{\alpha}{r'^2}\frac{1}{\sin\theta}\frac{\partial}{\partial\theta}\left(\sin\theta\frac{\partial T'}{\partial\theta}\right) \tag{7}$$

Now, the heat function, H', can be defined as:

$$\frac{1}{r^2\sin\theta}\frac{\partial H'}{\partial\theta}=\rho C V_r' T-k\frac{\partial T}{\partial r'} \tag{8}$$

(net energy flow in the radial direction)

$$-\frac{1}{r'\sin\theta}\frac{\partial H'}{\partial r'}=\rho C V_\theta' T-\frac{k}{r'}\frac{\partial T'}{\partial\theta} \tag{9}$$

(net energy flux in the azimuthal direction)

It can be readily seen that equations (8) and (9) identically satisfy the energy equation (7).

In order to compute the heat function $H'(r', \theta')$ in the flow field a Poisson-type partial differential equation was obtained from equations (8) and (9) in the following way.

Differentiate (8) with respect to θ, multiply r' to (9) and then differentiate it with respect to r'. Subtract the latter from the former to obtain the following heat function equation:

$$\frac{1}{\sin\theta}\frac{\partial^2 H'}{\partial r'^2}+\frac{1}{r'^2}\frac{\partial}{\partial\theta}\left(\frac{1}{\sin\theta}\frac{\partial H'}{\partial\theta}\right)=\rho C\left[\frac{\partial}{\partial\theta}(V_r'T)-\frac{\partial}{\partial\theta}(V_\theta' r' T)\right] \tag{10}$$

Equation (10) can be written in the non-dimensional form as:

$$\frac{1}{\sin\theta}\frac{\partial^2 H}{\partial r^2}+\frac{1}{r^2}\frac{\partial}{\partial\theta}\left(\frac{1}{\sin\theta}\frac{\partial H}{\partial\theta}\right)=\frac{Pe}{2(1-T_\infty)}\left[\frac{\partial}{\partial\theta}(V_r T)-\frac{\partial}{\partial r}(V_\theta r T)\right] \tag{11}$$

where

$$H=\frac{H'}{ka'(T_i-T_\infty)} \tag{12}$$

For the solutions of (1), (2), (6) and (11) the following boundary conditions[3] were utilized:

At free stream $(r\to\infty)$

$$\psi=\tfrac{1}{2}r^2\sin^2\theta+V_s(\cos\theta-1) \tag{13a}$$

$$\zeta=0 \tag{13b}$$

$$T=T_\infty \tag{13c}$$

$$-\frac{\partial H}{\partial r}=\frac{Pe}{2}\left(\frac{T_\infty}{1-T_\infty}\right)V_\theta r\sin\theta \tag{13d}$$

It is to be noted that the term containing V_s in boundary condition (13a) includes the effect of mass efflux so that the conservation of mass is satisfied within the domain. As r approaches ∞, (13a) automatically satisfies velocity relationships (4) and (5).

At the surface ($r = 1$)

$$\psi = V_s(\cos\theta - 1) \tag{14a}$$

$$\zeta = E^2\psi/\sin\theta \tag{14b}$$

$$T = 1 \tag{14c}$$

$$\frac{\partial H}{\partial r} = 0 \tag{14d}$$

Boundary condition (14d) is obtained from the fact that V_θ and $\partial T/\partial\theta$ are zero at the surface.

Axisymmetric conditions

At $\theta = 0$

$$\psi = 0 \tag{15a}$$

$$\zeta = 0 \tag{15b}$$

$$\frac{\partial T}{\partial\theta} = 0 \tag{15c}$$

$$\frac{\partial H}{\partial r} = \frac{\partial H}{\partial\theta} = 0 \tag{15d}$$

At $\theta = \pi$

$$\psi = -2V_s \tag{16a}$$

$$\zeta = 0 \tag{16b}$$

$$\frac{\partial T}{\partial\theta} = 0 \tag{16c}$$

$$\frac{\partial H}{\partial r} = \frac{\partial H}{\partial\theta} = 0 \tag{16d}$$

Values of H at $r = 1$ and $\theta = 0$ and π can be obtained from (8) by integrating it from $\theta = 0$ to π,

$$H(1, \pi) = PeV_s\left(\frac{1}{1 - T_\infty}\right) + Nu \tag{17}$$

where Nu is the conduction referenced Nusselt number and is given by:

$$Nu = -\frac{1}{1 - T_\infty}\int_0^\pi \left.\frac{\partial T}{\partial r}\right|_{r=1} \sin\theta\, d\theta \tag{18}$$

H at $r = 1$ and $\theta = 0$ is identically zero.

$$H(1, 0) = 0 \tag{19}$$

METHOD OF SOLUTION

Equations (1), (2), (6) and (11) were solved by the finite difference method using a point SOR scheme. For solving these equations the transformation $r = e^Z$ was introduced for the radial

Table 1 Comparison of characteristic parameters for thermal flow past a sphere

				C_D		Nu		
						Present model		
Re	*Pr*	Z_x	M × N	Present model	Eq. 20	3 pt.	4 pt.	Eq. 21
1	1	3.5	20 × 30	27.80	27.40	2.32	2.28	2.26
10	1	3	25 × 30	4.43 (4.40)	4.24	3.62	3.62 (3.59)	3.65
50	1	2.5	32 × 45	1.69 (1.65)	1.63	6.09	6.02 (6.01)	6.00
75	1	2.5	32 × 45	1.41	1.34	6.99	6.85	6.89
75	10	2.5	32 × 45			13.11	13.42	13.64
100	1	2.5	32 × 45	1.20 (1.187)	1.186	7.83	7.62 (7.70)	7.63

(Bracketed values of C_D and *Nu* are from Reference 10)

coordinate as suggested by several earlier workers[3,4,6,8] to obtain a denser mesh near the surface of the sphere, where the stream function, vorticity and temperature gradients are relatively large, and, hence, higher accuracy of the difference approximation is needed. For the solution of (1), (2) and (6), the external boundary was kept at a finite radial distance (r_∞) from the centre of the sphere in accordance with the Peclet number (*Pe*) being used, following the recommendation of the literature[3,4,6]. Constant step sizes in the radial (ΔZ) and angular ($\Delta\theta$) coordinates were used where they can be expressed as:

$$\Delta\theta = \pi/M, \qquad r_\infty = e^{Z_\infty} \qquad \text{and} \qquad \Delta Z = Z_\infty/N$$

where $M+1$ and $N+1$ are the number of mesh points in the angular and radial direction respectively. All the derivatives for (1) and (2) were expressed in central difference up to $Re = 100$. Relaxation factors for the solution of Ψ and ζ were kept at 1 and 0.1 respectivelt up to $Re = 50$. For Re above 50, relaxation factor for Ψ was kept at 1 whereas for ζ, it was reduced to 0.08. Details about the use of relaxation factors in the whole range of $1 < Re < 100$ can be found in References 4, 6.

For the solution of steady state energy equation (6) central differencing was applied with all the derivatives for solutions up to a maximum Peclet number of 100. But for *Pe* above 100, in order to increase the stability of the finite difference scheme, first order upwind differencing was introduced for the convective terms in (6). Symmetry boundary conditions were approximate with second order accuracy. A relaxation factor of 0.4 was used for $Pe < 10$. In the range of $10 \leqslant Pe \leqslant 50$, the relaxation factor was kept at 0.2 and in the range of $50 < Pe < 100$, it was kept at 0.08. With the use of upwind scheme the relaxation factor could be raised to 1.2. The energy equation (6) was solved for two levels of free stream temperature ($T_\infty = 0$ and 3). The tolerance limit for the convergence of the temperature field was kept at 10^{-5} from one iteration to the other. It may be noted that grid sizes as recommended by Abramzon and Elata[8] were chosen.

Before proceeding to solve the heat function equation (11), the accuracies of the ψ, ζ and temperature fields were tested through the drag coefficients, C_D (defined in Reference 5) and the Nusselt number according to equation (18). Reference values of C_D for a single sphere was taken from White[9] and the finite element solution of Ramachandran *et al.*[10], while the Nusselt number was taken from the empirical correlation of Clift *et al.*[11,10]. It can be worth mentioning here that while approximating temperature gradient on the sphere surface ($-\partial T/\partial r$) to compute *Nu*, the use of a four point formula was necessary because the standard three point differencing did not give correct values in some cases, as evident from *Tables 1* and *2*.

Table 2 Characteristic parameters for thermal flow past a sphere with surface blowing ($V_S = 0.2$)

				Nu (18)	
Re	*Pr*	Z_x	M × N	3 pt.	4 pt.
10	1	3	25 × 30	2.68	2.66
50	1	2.5	32 × 45	2.03	2.02
75	1	2.5	32 × 45	1.68	1.66
75	10	2.5	32 × 45	−0.268	0.347
100	1	2.5	32 × 45	1.41	1.39

The heat function θ, equation (11), was solved by a point SOR scheme after expressing (11) in a finite difference form. The standard space centred differencing was used for all the terms in (11). The right hand side of (11) behaves as the source term because all the parameters in it are predetermined from the solution of velocity and temperature field. Relaxation factor used for the solution of (11) was kept at 1.75 up to a *Pe* of 50. In the range of $50 \leqslant Pe \leqslant 100$, the relaxation factor was kept at 1.2 and beyond this range, it was kept at 0.8. The H field was assumed to have reached convergence when the maximum spatial deviation in H, over the whole domain of computation was below 10^{-6} from one iteration to the other.

RESULTS AND DISCUSSION

Nusselt number – an input to the H *field*

It can be seen from (17) that *Nu* is required to fix the values of H at $r = 1$ and $\theta = \pi$. In fact this value of H remains constant on the line $\theta = \pi$ because $\partial N/\partial r = 0$ on this line and similarly on $\theta = 0$, H remains at zero. The values of *Nu* tabulated in *Tables 1* and *2* are input to the computation of H field and hence, it is essential that these values are accurately computed.

In the method of solution it is indicated that the accuracy of the flow field and the temperature field have been verified through the drag coefficient C_D (as defined in References 5, 9) and the Nusselt number *Nu*. The drag coefficient for a single sphere according to White[10] and the Nusselt number according to Clift *et al.*[11] are expressed as:

$$C_D = \frac{24}{Re} + \frac{6}{1+\sqrt{Re}} + 0.4 \tag{20}$$

(for $1 < Re < 2 \times 10^5$)

$$\frac{Nu - 1}{Pr^{1/3}} = \left[1 + \frac{1}{Re \cdot Pr}\right]^{1/3} Re^{0.41} \tag{21}$$

(for $1 < Re < 400$, $0.25 < Pr < 100$)

The values of C_D and *Nu* are tabulated for various *Re* in the *Table 1*, for the case of no mass efflux on the sphere surface. It can be observed that our present computations agree very well with those of (20) and (21) as well as with the numerical (finite element) calculations of Ramachandran *et al.*[10]. Particularly for the case of $Re = 50$, 75 and 100 a four point approximation to compute *Nu*, gives a better comparison with those of literature[10,11].

Table 2 shows the conduction referenced Nusselt number for the sphere when there is a constant radial mass efflux, present at the surface. For this case, it can be observed that the *Nu*

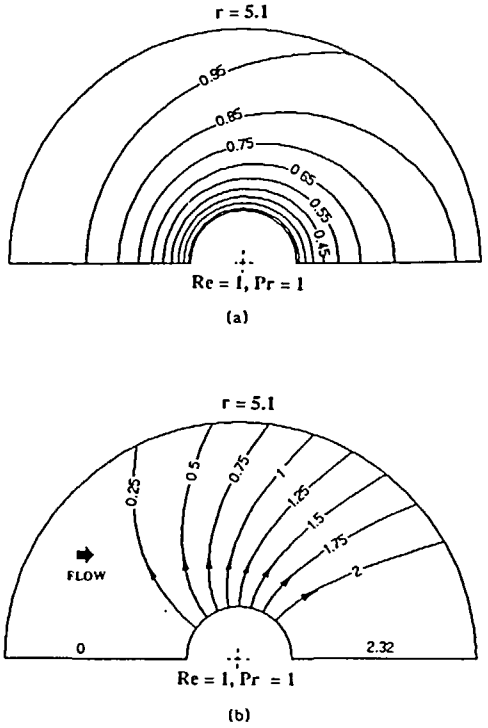

Figure 2 Isotherms and heat lines around a solid sphere subjected to cooling

values decrease with *Re* when the non-dimensional mass efflux remains constant at $V_s = 0.2$. It is also worth mentioning that *Nu* at a particular *Re* decreases with the existence of radial mass efflux, which is very similar to the case of an evaporating drop. When there is a radial mass efflux at the surface of the sphere, the thermal boundary layer becomes thicker compared to the case of no mass efflux. Hence the temperature gradient on the sphere decreases compared to a no mass efflux situation and therefore, the Nusselt number decreases. As Re increases for a constant sphere diameter, the free stream velocity also increases and the surface blowing becomes stronger even though the non-dimensional radial velocity at the surface (V_s) remains fixed at 0.2, because the reference velocity here is the free stream velocity. The stronger is the surface blowing, the thicker is the thermal boundary layer and the lower is the value of Nu. This is the reason why Nu falls with Re when the radial mass efflux remains constant. Again in *Table 2* it can be seen that for the case of $Re = 75$, the use of a three point formula to compute Nu, gives an unrealistic value, while the four point formula does not.

Visualization of energy flow

Now, coming back to the visualization of convective heat transfer let us presently concentrate at *Figure 2*. In *Figure 2a* the local temperature field around the sphere is plotted in terms of isotherms up to a radius of $5.1a'$, for the case of $Re = 1$ and $T_\infty = 0$. In *Figure 2b* the corresponding heat lines are shown which are starting normal to the sphere surface. The *H* lines are almost orthogonal to the isotherms in *Figure 2a*, for this Re, because for a low value of Re convection component of heat transfer is almost negligible in comparison to the conduction counterpart.

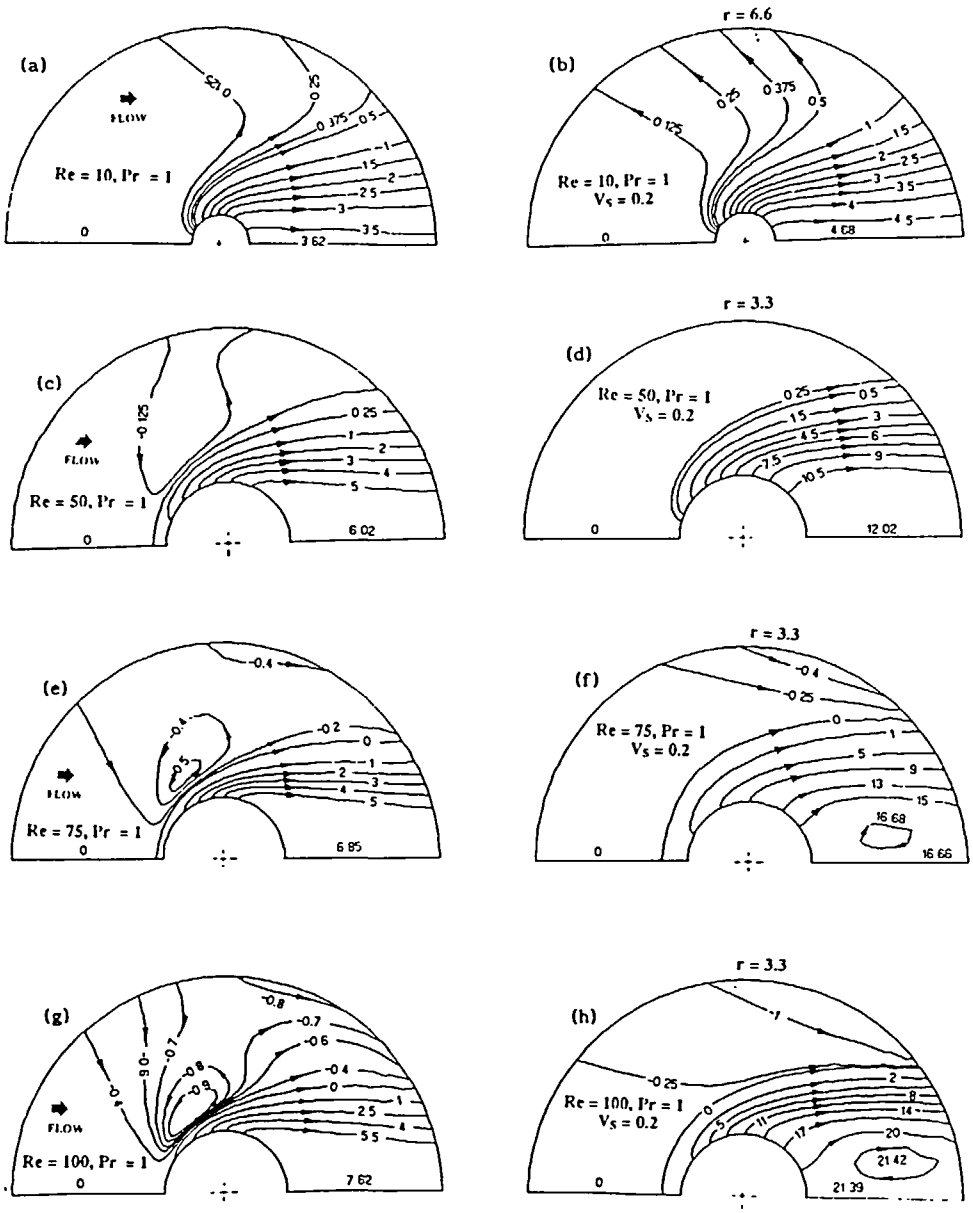

Figure 3 Visualization of heat line around a solid sphere with and without radial mass efflux for different Re with $Pr = 1$ fluid

The radial curved heat lines show the direction of energy flow from the sphere to the free stream ambience, which is at a low temperature compared to the sphere.

Figure 3 shows the comparison of energy flow from the sphere for the case of $V_s = 0$ (no surface blowing) and $V_s = 0.2$, with $Re = 10$, 50, 75 and 100, while the free stream temperature T_∞ is set to be zero. The sphere is being cooled here and the energy plume rising from the surface of the sphere can be easily seen. The difference of H values between any two $H =$ constant lines is

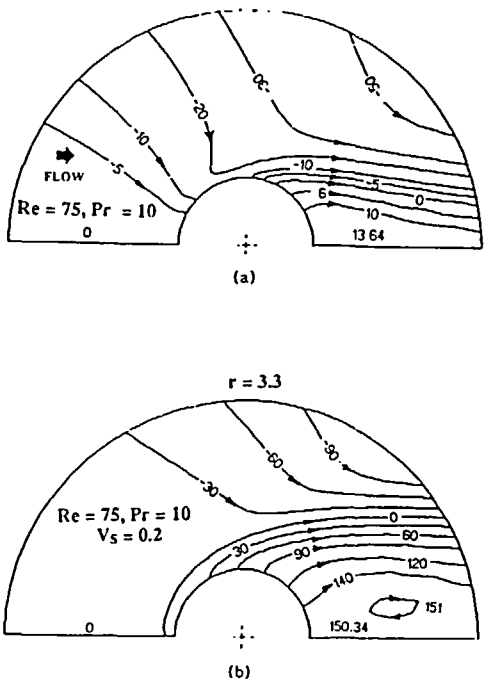

Figure 4 Comparison of energy flow around a sphere with and without surface blowing for a $Pr = 10$ fluid

proportional to the energy flow between those two lines. It can be observed from *Figure 3* ($Re = 10$ case) that the amount of energy flowing between the lines $H = 0$ and $H = 0.125$, passes through a larger surface area compared to the case of the surface blowing (at same Re). When there is surface blowing, much of the energy is carried away by convection transport and hence through a smaller area large amount of energy can pass through. This fact is visualized in all the cases of Re ranging from 10 to 100. As Re increases the hydrodynamic and the thermal boundary layers become thin and energy transport from the sphere to the ambience occurs through a thinner surface area. For the case of $Re = 75$, $H = 0$ line starts very close to the front stagnation point of the sphere and for $Re = 100$, it starts from the top of the sphere almost at an angle of $\theta = 30°$. But with the presence of radial mass efflux the $H = 0$ line shifts to the left, which seems to be very logical, it can also be observed from *Figure 3* that with the presence of a radial mass efflux the energy plume rises a little bit from the surface of the sphere before it is carried away by the surrounding fluid when compared to its non-blowing counterpart.

From *Figure 4* a comparison between the characteristics of energy flow for the case of a high Pr number can be drawn to that of a low Pr number case when the sphere is being cooled by the surrounding fluid ($T_\infty = 0$). In *Figure 4a* negative heat lines are meeting the surface of the sphere and $\partial H/\partial\theta$ is negative for $\theta < 90°$. This suggests that the front half of the sphere is receiving energy from the ambient while the rear half of the sphere is releasing energy to the ambient where $\partial H/\partial\theta$ is positive. This looks something different from our conventional thinking, but this is logical and an explanation to this will be made later. Such type of energy flow does not take place in the case of a low Pr number (*Figure 3f*) where the entire sphere is releasing energy to the ambient. In *Figure 4b* with the association of a radial mass efflux the picture of the energy flow changes entirely. Here the entire sphere is releasing energy to the surrounding fluid like its counterpart in *Figure 3f*.

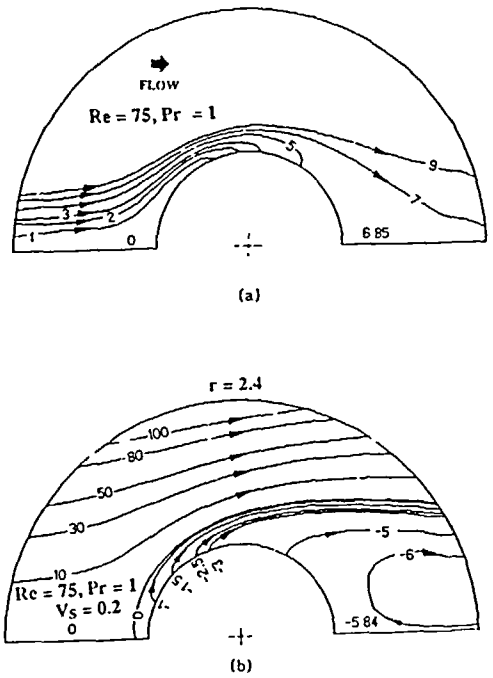

Figure 5 Heat lines around a solid sphere subjected to heating by a high temperature fluid flow

Figure 5 represents the case of a sphere being heated by the surrounding fluid. As a test case T_∞ is chosen as 3. Here energy is carried from the free stream (*Figure 5a*) and is fed to the sphere. In the front half of the sphere $\partial H/\partial\theta$ is positive, suggesting that energy flow is almost radially outward. Due to the non-dimensional scheme of (12) H becomes negative because of the fact that $T_\infty > T_i$. So the actual energy flow will be towards the sphere and the arrows are shown in its true sense to avoid confusion. But in *Figure 5b* the sphere is subjected to a case of heating by the surrounding fluid with the existence of a surface mass efflux and it so happens that energy goes away from the sphere instead of coming to it. Hence the sphere instead of being heated is being cooled and an explanation to this situation can be made in the following way. In the rear half of the sphere (*Figure 5b*), i.e.: for $\theta > 90°$, the direction of velocity is away from the sphere. Energy flow in the flow field consists of two parts, one being the convection and the other conduction. Due to the high temperature surrounding fluid conduction heat transfer will be radially in while the convective heat transfer will be radially out. So, a race between the two modes of heat transfer takes place and where convection dominates over conduction the net energy flow takes the direction of convection. The same reason is applicable to the case of *Figure 4a* where the front portion of the sphere receives energy from the flow field even though the surrounding fluid is at a low temperature compared to that of the sphere.

CONCLUSIONS

A heat function, similar to that of a stream function, has been introduced in the spherical polar coordinate system to visualize the direction of energy flow around a sphere when the sphere is either heated or is being cooled. Solutions of the steady state momentum and energy equation

have been obtained numerically around the sphere up to a maximum Reynolds number of 100 and *Pe* number of 750 to visualize the energy interaction between the surrounding fluid and that of the sphere. It has been shown that there exists zones in the flow field which do not interact with the sphere so far as energy exchange with the sphere is concerned. It has also been established that the sphere can receive energy from the ambient fluid even if the ambient is at a low temperature compared to that of the sphere. This phenomenon of energy interaction with the sphere would not have been possible to visualize without the construction of the heat function or the heat lines. Hence, it is felt that the heat lines give more insight to the understanding of energy flow in convection heat transfer compared to the standard isotherm plots.

ACKNOWLEDGEMENTS

The authors are grateful to Director, CMERI for supporting this work.

REFERENCES

1 Kimura, S. and Bejan, A. Heat line visualization of convective heat transfer, *ASME J. Heat Transfer*, **105**, 916–919 (1983)
2 Bejan, A. *Convection Heat Transfer*, John Wiley & Sons (1984)
3 Hamielec, A. E., Hoffman, T. W. and Ross, L. L. Numerical solution of the Navier-Stokes equation for the flow past spheres: Part I viscous flow around spheres with and without radial mass efflux, *AIChE J.* **13**, 212–219 (1967)
4 LeClair, B. P., Hamielec, A. E. and Pruppacher, H. R. A numerical study of the drag on a sphere at low and intermediate Reynolds number, *J. Atmospheric Sci.*, **27**, 308–315 (1970)
5 Dash, S. K. *Numerical modeling and thermodynamic studies on evaporation and combustion of liquid droplets and sprays*, Ph.D. Thesis, Indian Institute of Technology, Kharagpur (1989)
6 Dash, S. K., Sengupta, S. P. and Som, S. K. Transport processes and associated irreversibilities in droplet evaporation, *AIAA J. Thermophysics and Heat Transfer*, **5**, 366–373 (1991)
7 Kays, W. M. and Crawford, M. E. *Convective Heat Transfer*, 2nd ed., McGraw-Hill, New York (1980)
8 Abramzon, B. and Elata, C. Unsteady heat transfer from a single sphere in Stokes flow, *Int. J. Heat Mass Transfer*, **27**, 687–695 (1984)
9 White, F. M., *Viscous Fluid Flow*, McGraw-Hill, New York (1974)
10 Ramachandran, R. S., Kleinstreuer, C. and Wang, T.-Y. Forced convection heat transfer of interacting spheres, *Num. Heat Transfer, Part A*, **15**, 471–487 (1989)
11 Clift, R., Grace, J. R. and Weber, M. E. *Bubbles, Drops and Particles*, Academic Press, New York (1978)